Pressure-induced permanent metallization with reversible structural transition in molybdenum disulfide

YuKai Zhuang, LiDong Dai, Lei Wu, HePing Li, HaiYing Hu, KaiXiang Liu, LinFei Yang, and Chang Pu

Citation: Appl. Phys. Lett. **110**, 122103 (2017); doi: 10.1063/1.4979143
View online: https://doi.org/10.1063/1.4979143
View Table of Contents: http://aip.scitation.org/toc/apl/110/12
Published by the American Institute of Physics

Pressure-induced permanent metallization with reversible structural transition in molybdenum disulfide

YuKai Zhuang,[1,2] LiDong Dai,[1,a)] Lei Wu,[1] HePing Li,[1] HaiYing Hu,[1] KaiXiang Liu,[1,2] LinFei Yang,[1,2] and Chang Pu[1,2]
[1]*Key Laboratory of High-Temperature and High-Pressure Study of the Earth's Interior, Institute of Geochemistry, Chinese Academy of Sciences, Guiyang, Guizhou 550081, People's Republic of China*
[2]*University of Chinese Academy of Sciences, Beijing 100039, People's Republic of China*

(Received 3 December 2016; accepted 13 March 2017; published online 22 March 2017)

This report presents a pressure-induced permanent metallization for MoS_2 under non-hydrostatic conditions. Impedance and Raman spectra were measured to study the pressure-induced structural and electronic transformations of MoS_2 at up to ~25 GPa in diamond anvil cells under both non-hydrostatic and hydrostatic conditions. The results show evidence for isostructural hexagonal distortion from 2*Hc* to 2*Ha* and metallization at ~17 GPa and ~20 GPa under non-hydrostatic and hydrostatic conditions, respectively. Interestingly, the metallization is irreversible only under non-hydrostatic compression. We attribute this phenomenon to the incorporation of molecules of pressure medium between layers, which mitigate compressed stress and reduce interlayer interaction. *Published by AIP Publishing*. [http://dx.doi.org/10.1063/1.4979143]

Recently, with the discovery of graphene,[1] two-dimensional (2D) materials have been received increasing attention, especially the layered transition metal dichalcogenides (LTMD).[2,3] As a typical LTMD, MoS_2 has motivated intensive interest in fields such as lubricants,[4] photovoltaics,[5] and transistors.[6] Unlike graphene,[7] bulk and monolayer MoS_2 are semiconductors with an indirect band gap of 1.23 eV and a direct band gap of 1.8 eV, respectively.[8,9] Its tunable semiconducting behavior makes it a tremendously promising material for transistors and other electronic devices.[8,9]

In monolayer MoS_2, one metal atom (Mo) plane is sandwiched by two chalcogen atom (S) planes, forming a trigonal prismatic coordination.[10] And the MoS_2 layers are interconnected by the d-orbital states of the Mo atoms with van der Waals forces.[11] Different layer stacking patterns form a variety of crystal structures, like the 2*Ha* and 2*Hc* structure.[12] It has been demonstrated that chemical doping,[13] intercalation,[14] and surface functionalization[15] can change the structure of MoS_2. As one effective approach, pressure can induce the isostructural hexagonal distortion of MoS_2.[7,16,17] Furthermore, the transition pressure points have been obtained by theoretical calculations and experimental studies.[7,12,18] It is generally believed that the structural transition occurs simultaneously with metallization. For most LTMDs, the closure of the interlayer Van der Waals gap is accompanied by structural reorganization and atomic displacement, resulting in a first-order structural phase transition.[15,19] However, a recent study on $MoSe_2$ has found that metallization occurs under high pressure without any structural phase transition.[20] This indicates that the overlap of the conduction and valence bands is the key factor in inducing metallization, instead of the structural phase transition.[20] In another recent study, WS_2 was shown to undergo a structural phase transition (2*Hc* to 2*Ha*) and metallization at around 37 GPa owing to the strong shear stress caused by non-hydrostatic conditions.[21] However, the corresponding structural transition disappeared when He was used as a pressure medium owing to the insertion of He atoms into the WS_2 layers.[21] In other words, the use of pressure media greatly affects the properties of layered materials under high pressure. Experimental evidence for the influence of non-hydrostatic conditions on the structural transition and metallization of MoS_2 is still absent.[7,16,18,22] Based on this, there are several interesting and unresolved questions for MoS_2: (i) What is the relationship between structural transition and metallization? (ii) What is the effect of pressure media on the properties of MoS_2? In this study, we explored the properties of MoS_2 under non-hydrostatic and hydrostatic conditions. The results showed that the structural transition and metallization of MoS_2 are reversible under hydrostatic conditions. However, under non-hydrostatic conditions, the structural transition is reversible, but is accompanied by permanent metallization.

MoS_2 powder samples (Aladdin, China) were commercially purchased for this study. Under ambient conditions, X-ray diffraction analysis revealed that the samples belonged to hexagonal *mmc* space group (2*H*-MoS_2) with the following lattice parameters: $a = b = 3.165$ Å, $c = 12.318$ Å, $\alpha = \beta = 90°$, $\gamma = 120°$, which is consistent with previous studies.[7,16,18] Atomic force microscopy (AFM) and transmission electron microscopy (TEM) images were obtained using a Multimode 8 mass spectrometer (Bruker) and Tecnai G2 F20 S-TWIN TMP, respectively. Raman and electrical experiments were carried out using a 300 μm culet diamond anvil cell (DAC). Pressure was calibrated through the wave number shift of ruby fluorescence.[23] Raman spectra were collected using a Micro-Confocal Spectrometer in quasi-backscattering geometry. For hydrostatic conditions, a mixture of methanol and ethanol in 4:1 volume ratio was chosen as the pressure media. No pressure medium was used under non-hydrostatic conditions. The high pressure electrical conductivity of the samples was measured using a Solartron-1260 AC impedance spectroscopy

a)Email: dailidong_2014@hotmail.com

analyzer. Details of the measurement procedures were presented in our previous work.[24]

Representative Nyquist plots of the impedance of MoS_2 at different pressures up to ~25 GPa under non-hydrostatic conditions are shown in Fig. 1. The semi-circular arc in the high frequency region of Fig. 1(a) corresponds to a bulk contribution, while the semi-circle in the low frequency region on the right represents the grain boundary contribution.[25] The plots were fitted with Z-View software with an error of less than 5%. Both semicircular arcs gradually decreased and the grain boundary resistance disappeared at around 7.5 GPa. At higher pressure, the impedance spectra only appeared in the fourth quadrant, which represents the electronic response of the sample (Fig. 1(b)).[26]

The equivalent circuit of Fig. 1(a) consists of two parts, each including a resistor and a constant phase element (R-CPE) in parallel. To confirm the validity of the fitting results, the corresponding fitting curves are also shown in Fig. 1(a). Meanwhile, the equivalent circuit of Fig. 1(b) was taken as a simple resistor. The value was obtained for $Z'' = 0$ and the influence of the wire resistance was considered.[27]

The upper-left illustration of Fig. 1(a) shows the ratio between the grain boundary and grain interior resistance. The grain boundary resistance was greater than the grain interior resistance by about sixteen orders of magnitude under ambient conditions. As the pressure was increased, the ratio gradually decreased and became zero until ~7.5 GPa. This phenomenon indicates that the electronic crystal structure of the MoS_2 changed greatly in this pressure range, and demonstrated a pressure induced electronic polarization[28] caused by the increasing width of the grain boundaries along the direction of current transmission.[29]

Fig. 2(a) shows the pressure-dependent conductivity of MoS_2 at room temperature. With increasing pressure, the conductivity of MoS_2 was gradually enhanced until ~7.5 GPa and then abruptly increased by about three orders of magnitude between ~7.5 and ~17 GPa, in good agreement with the previous results of Nayak *et al.*[16] With further compression to about ~25 GPa, the conductivity tended to stabilize between ~0.5 and ~0.8 S cm^{-1}. The sudden change in conductivity with respect to pressure at ~17 GPa is in accordance with the characteristics of a first-order structural transition.[16] Additionally, the orders of magnitude change in conductivity up to ~25 GPa indicates that the MoS_2 may have been metallized.[16,22] As shown in Fig. 2(a), the observed variation in conductivity with pressure could be divided into three distinct regions: (i) semiconducting area up to ~7.5 GPa (SC), (ii) intermediate state between semiconductor and metal from ~7.5 to ~17 GPa (IS), and (iii) metallic zone above ~17 GPa. Upon decompression, the conductivity of MoS_2 decreased very slowly and reached $\sim 1 \times 10^{-1}$ S cm^{-1} at atmospheric pressure. Furthermore, even with a much longer relaxing time (72 h), the conductivity of the decompressed sample remained $\sim 1 \times 10^{-1}$ S cm^{-1}.[30] This irreversible metallization is an enormous difference with previous results.[16,17,22] Therefore, to verify this permanent metallization in MoS_2, we performed in situ temperature-dependent conductivity measurements.

The conductivity of a semiconductor increases with increasing temperature, while that of the metal does the opposite.[16,22] As can be seen from Figs. 2(b) and 2(c), under non-hydrostatic conditions the conductivity of MoS_2 increased with temperature at ~10 GPa, which is a typical semiconductor property. Conversely, the conductivity decreased with increasing temperature at ~25 GPa and upon decompression, a typical metallic behavior. However, in Fig. 2(d), the conductivity vs. temperature curves show semiconducting behaviors both at ~10 GPa and upon decompression under hydrostatic conditions.

Our experimental results distinctly show the reversible and irreversible metallization of MoS_2 under two types of pressure conditions. A reasonable explanation for the different properties displayed by MoS_2 under non-hydrostatic and hydrostatic conditions is the influence of pressure media and anisotropic stress. The overlap of the conduction band and valence band resulting from the decrease in interlayer spacing caused by compressive stress is the crucial factor in the metallization of MoS_2.[17,31] For hydrostatic conditions, the molecular dynamic diameters of methanol and ethanol are 0.38 nm and 0.43 nm, respectively, while the interlayer spacing of MoS_2 is ~6.5 nm.[16] This means that the molecules of methanol and ethanol can enter the interlayer space to alleviate the interlayer interactions. After decompression, the layer spacing recovers with the escape of methanol and ethanol molecules.[32] For the non-hydrostatic sample, a stronger interaction is generated in the van der Waals gap, preventing the recovery of the interlayer spacing after compression owing to the absence of methyl alcohol molecules and the presence of strong anisotropic stress.[33,34] In fact, another recent study has also confirmed that the pressure medium is a significant factor

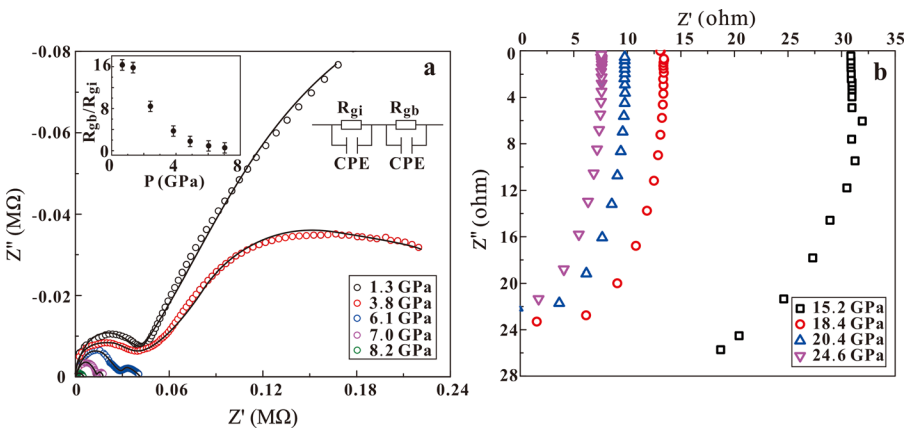

FIG. 1. Selected impedance spectra (Nyquist plots) in the complex plane of MoS_2 at different pressures. Inset: Grain boundary/grain interior resistance (R_{gb}/R_{gi}) versus pressure. This ratio represents the dominance of the grain boundary or grain interior resistance in the conduction process.

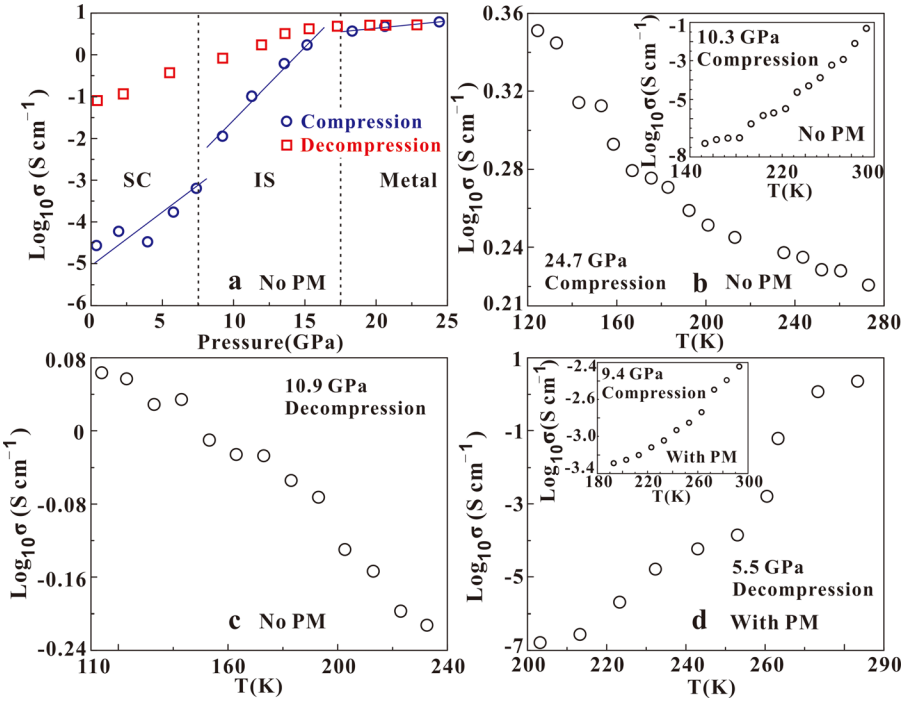

FIG. 2. The electronic properties of MoS_2. (a) Pressure-dependent electrical conductivity of MoS_2 under non-hydrostatic conditions. (b) and (c) Temperature-dependent conductivity of MoS_2 under non-hydrostatic conditions. (d) Temperature-dependent conductivity of MoS_2 under hydrostatic conditions with pressure media (PM).

in determining the stability of layered structures.[21] More importantly, stronger interlayer interactions can perhaps change the electronic structure permanently.

To determine the relationship between structural transition and irreversible metallization, high-pressure Raman spectral studies were carried out under non-hydrostatic and hydrostatic conditions, and the results are displayed in Fig. 3. Four typical Raman vibration modes for MoS_2 were observed at room pressure: E_{1g} (286 cm^{-1}), $E^1{}_{2g}$ (383 cm^{-1}), A_{1g} (409 cm^{-1}), and $E^2{}_{2g}$ (32 cm^{-1}).[35,36] A_{1g} is the interlayer vibration mode, while the others are intra-layer vibration modes.[37] In the non-resonant condition, A_{1g} and $E^1{}_{2g}$ are the two dominant vibrational modes.[38] Fig. 3(a) shows the representative Raman spectra of MoS_2 under non-hydrostatic conditions, in which the two dominant Raman modes exhibited a systematic blue shift with increasing pressure. In Fig. 3(b), the Raman shift rate of the A_{1g} mode with pressure was significantly higher than that of the $E^1{}_{2g}$ mode, which

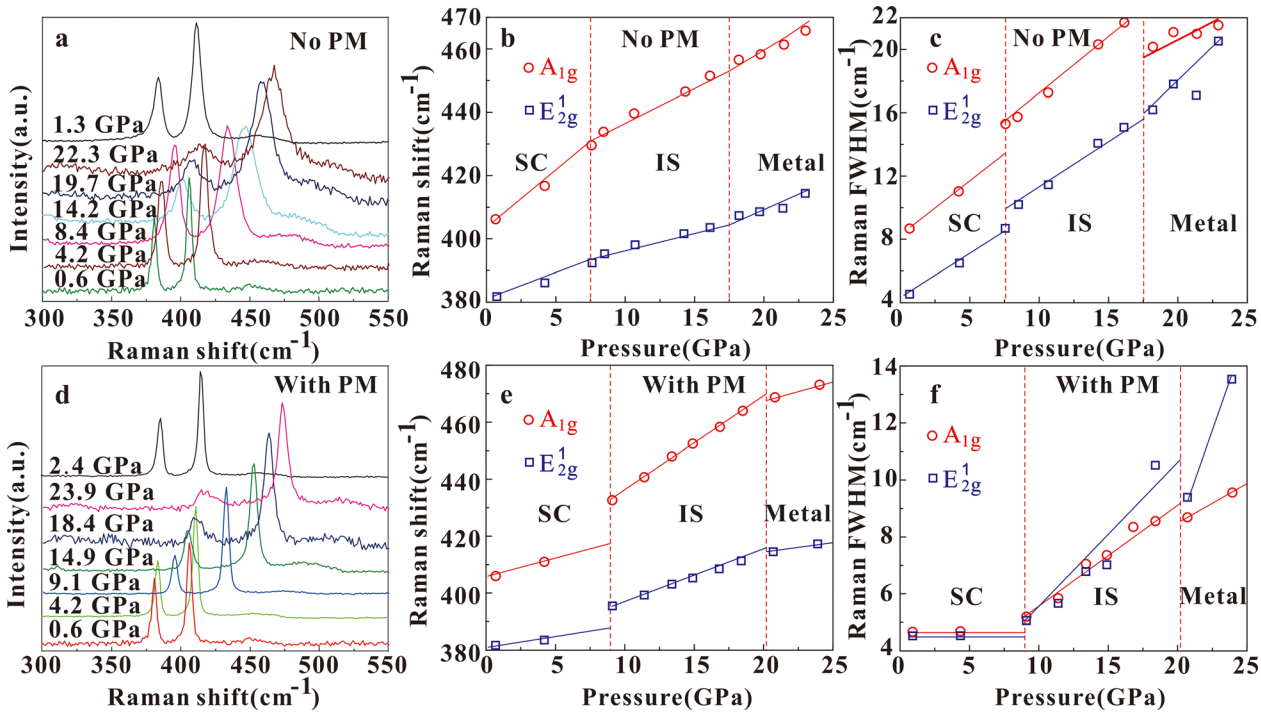

FIG. 3. Raman spectra of MoS_2 under high pressure. (a) and (d) Raman spectra at representative pressure points under non-hydrostatic and hydrostatic conditions, respectively. (b) and (e) Raman shifts of A_{1g} and $E^1{}_{2g}$ Raman modes with increasing pressure under non-hydrostatic and hydrostatic conditions, respectively. The straight lines serve as visual guides. (c) and (f) Raman FWHM for the two modes with increasing pressure under non-hydrostatic and hydrostatic conditions, respectively. The straight lines serve as visual guides.

indicates that the A_{1g} mode was more strongly affected by pressure. Specifically, E^1_{2g} mode is less susceptible to pressure owing to the strong covalent bond. In contrast, the A_{1g} mode corresponding to the interlayer atomic vibration is susceptible to the volumetric compression and interlayer slip under high pressure because of the weak van der Waals force. Additionally, the two abrupt transition points of the A_{1g} and E^1_{2g} modes with pressure (at ~7.5 and ~17 GPa) are in a good agreement with the variation in conductivity with pressure. Besides, as seen in Fig. 3(c), the pressure dependence of the full-width at half-maximum (FWHM) was similar to that of the Raman spectral shifts, which apparently indicates an increase in lattice anharmonic vibration.[16] Therefore, it was confirmed through Raman and impedance spectroscopy that isostructural hexagonal distortion from 2*Hc* to 2*Ha*[12] and metallization[7,16,17] of the MoS_2 occurred at ~17 GPa in non-hydrostatic conditions.

Under hydrostatic conditions, as shown in Figs. 3(e) and 3(f), the pressure dependence of the Raman spectral shifts and FWHM exhibited similar variations to those observed under non-hydrostatic conditions except for the delay in the transition points, which occurred at higher pressures of around 9 and 20 GPa. The discrepancy can be attributed to the effect of anisotropic stress under non-hydrostatic conditions, which leads to stronger compressibility and increased bulk modulus.[39] Additionally, the Raman modes of the MoS_2 returned to their initial state upon decompression under both non-hydrostatic and hydrostatic conditions, indicating that the structural transition is reversible (Figs. 3(a) and 3(b)).[17] Raman spectroscopy is sensitive to lattice vibration,[32] and the isostructural hexagonal distortion of MoS_2 is caused by interlayer slipping owing to tensile stress.[17,31] This interlayer sliding of MoS_2 is reversible upon decompression under both non-hydrostatic and hydrostatic conditions, and is therefore reflected in the Raman spectra.

AFM and TEM are effective methods for exploring small changes in morphology and interlayer spacing. Therefore, we carried out AFM and TEM studies to support the hypothesized conclusions. As seen in Figs. 4(a) and 4(b), the layered structure of MoS_2 under hydrostatic conditions was well preserved upon decompression from 24.4 GPa. However, upon decompression under non-hydrostatic conditions from 23.9 GPa, the surface morphology of the MoS_2 was completely destroyed and became lumpy, which means that MoS_2 has a limited tolerance to anisotropic stress and is significantly affected by it without the protection of a pressure medium. In fact, a similar phenomenon regarding the irreversible phase transition has been found for $LiMn_2O_4$ using scanning electron microscopy.[40] Furthermore, the TEM images (Figs. 4(c) and 4(d)) show that the initial interlayer spacing of the MoS_2 was ~0.65 nm.[41] It then became ~0.18 nm upon decompression from 25.3 GPa under non-hydrostatic conditions and ~0.45 nm upon decompression from 24.8 GPa under hydrostatic conditions. Additionally, the layered structure of the sample was partially destroyed only under non-hydrostatic conditions. This means that the change in interlayer spacing was irreversible under non-hydrostatic conditions. In contrast, the molecules of the pressure medium entered the interlayer spacing, which weakened the interlayer interactions and caused the change in spacing to be reversible under hydrostatic conditions. All of the above results therefore confirm that MoS_2 undergoes irreversible metallization only under non-hydrostatic conditions.

Previous studies on MoS_2 revealed its continuous lattice contraction under pressure with a c-axis compression ratio 2–3 times larger than that of the a-axis and b-axis.[16,18] Under non-hydrostatic conditions MoS_2 is subjected to more intense effects under pressure and greater interlayer interactions, which leads to the irreversible metallization. More

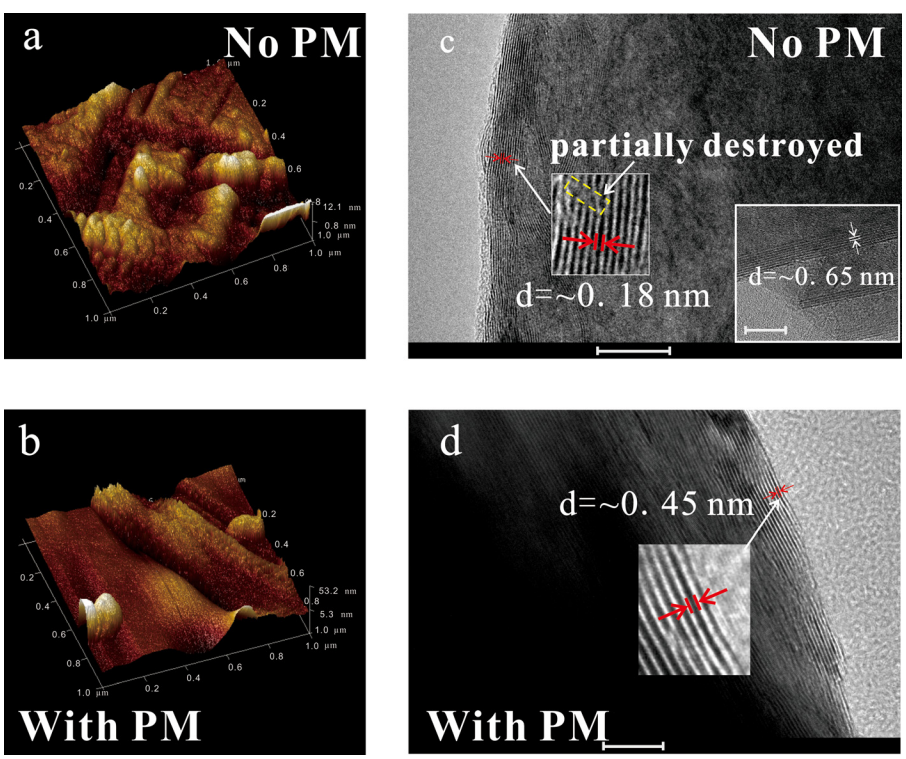

FIG. 4. (a) and (b) AFM images of pressure-induced morphology of MoS_2 upon decompression from 23.9 GPa under non-hydrostatic conditions and 24.4 GPa under hydrostatic conditions, respectively. (c) and (d) TEM images of MoS_2 upon decompression from 25.3 GPa under non-hydrostatic conditions and 24.8 GPa under hydrostatic conditions, respectively. Scale bars are 20 nm and 10 nm, respectively. Inset: TEM image of the initial sample. Scale bar, 10 nm.

generally, stronger interlayer interactions produce more intense attraction between two adjacent layers and are more likely to generate a sustained lattice response in extreme environments such as high pressure.

Previous studies have also reported changes in electronic properties from insulating or semiconducting to a metallic state for some 2D materials.[42–44] In these materials, the changes in electronic properties and the closure of their energy gap are generally accompanied by structural transitions. The transformation of electronic properties tends to be reversible as the structure recovers upon decompression. However, in the present work, the metallization of MoS_2 is not reversible with the recovery of the structure under non-hydrostatic conditions. Additionally, the non-hydrostatic pressure induced irreversible metallization may be derived from the special band structure of MoS_2 and its defective electronic state. This may be better applied in materials science in future, and many other LTMDs may also exhibit similar properties.

In summary, the structures, vibrations, and electronic properties of MoS_2 under high pressure have been systematically studied by high-pressure Raman spectroscopy, impedance spectroscopy, atomic force microscopy, transmission electron microscopy, and temperature-dependent conductivity measurements. In this study, MoS_2 underwent an isostructural hexagonal distortion from $2Hc$ to $2Ha$ at ~17 GPa under non-hydrostatic conditions accompanied by an electronic transition from semiconductor to metal. The reversible structural transition and metallization of MoS_2 occurred under hydrostatic conditions. However, under non-hydrostatic conditions the metallization was irreversible. We emphasize the key role of pressure media in reducing interlayer interaction during compression and restoring the interlayer spacing upon decompression. The structural and electronic properties of MoS_2 are a unity of opposites, and may have potential applications in opto-electronics and photovoltaic devices.

This research was financially supported by the Strategic Priority Research Program (B) of the Chinese Academy of Sciences (XDB 18010401), Key Research Projects of the Frontier Science of the Chinese Academy of Sciences (QYZDB-SSW-DQC009), "135" Program of the Institute of Geochemistry of CAS, Hundred Talents Program of CAS, NSF of China (41474078, 41304068, and 41174079), and the Special fund of the West Light Foundation of CAS.

[1]K. S. Novoselov, A. K. Geim, S. V. Morozov, D. Jiang, Y. Zhang, S. V. Dubonos, I. V. Grigorieva, and A. A. Firsov, Science **306**, 666 (2004).
[2]E. Benavente, M. A. Santa Ana, F. Mendizabal, and G. Gonzalez, Coord. Chem. Rev. **224**, 87 (2002).
[3]H. Zeng, J. Dai, W. Yao, D. Xiao, and X. Cui, Nat. Nanotechnol. **7**, 490 (2012).
[4]Z. Chen, X. Liu, Y. Liu, S. Gunsel, and J. Luo, Sci. Rep. **5**, 12869 (2015).
[5]K. F. Mak, C. Lee, J. Hone, J. Shan, and T. F. Heinz, Phys. Rev. Lett. **105**, 136805 (2010).
[6]B. Radisavljevic, A. Radenovic, J. Brivio, V. Giacometti, and A. Kis, Nat. Nanotechnol. **6**, 147 (2011).
[7]N. Bandaru, R. S. Kumar, D. Sneed, O. Tschauner, J. Baker, D. Antonio, S. N. Luo, T. Hartmann, Y. S. Zhao, and R. Venkat, J. Phys. Chem. C **118**, 3230 (2014).
[8]K. K. Kam and B. A. Parklnson, J. Phys. Chem. **86**, 463 (1982).
[9]A. Splendiani, L. Sun, Y. Zhang, T. Li, J. Kim, C. Y. Chim, G. Galli, and F. Wang, Nano Lett. **10**, 1271 (2010).
[10]M. Dave, R. Vaidya, S. G. Patel, and A. R. Jani, Bull. Mater. Sci. **27**, 213 (2004).
[11]A. Ayari, E. Cobas, O. Ogundadegbe, and M. S. Fuhrer, J. Appl. Phys. **101**, 014507 (2007).
[12]X. Fan, D. J. Singh, Q. Jiang, and W. T. Zheng, Phys. Chem. Chem. Phys. **18**, 12080 (2016).
[13]B. Radisavljevic and A. Kis, Nat. Mater. **12**, 815 (2013).
[14]G. Eda, H. Yamaguchi, D. Voiry, T. Fujita, M. Chen, and M. Chhowalla, Nano Lett. **11**, 5111 (2011).
[15]E. Arcangeletti, L. Baldassarre, D. Di Castro, S. Lupi, L. Malavasi, C. Marini, A. Perucchi, and P. Postorino, Phys. Rev. Lett. **98**, 196406 (2007).
[16]A. P. Nayak, S. Bhattacharyya, J. Zhu, J. Liu, X. Wu, T. Pandey, C. Jin, A. K. Singh, D. Akinwande, and J. F. Lin, Nat. Commun. **5**, 3731 (2014).
[17]X. Zhang, X. F. Qiao, W. Shi, J. B. Wu, D. S. Jiang, and P. H. Tan, Chem. Soc. Rev. **44**, 2757 (2015).
[18]R. Aksoy, Y. Ma, E. Selvi, M. C. Chyu, A. Ertas, and A. White, J. Phys. Chem. Solids **67**, 1914 (2006).
[19]C. Ataca and S. Ciraci, J. Phys. Chem. C **115**, 13303 (2011).
[20]Z. Zhao, H. Zhang, H. Yuan, S. Wang, Y. Lin, Q. Zeng, G. Xu, Z. Liu, G. K. Solanki, K. D. Patel, Y. Cui, H. Y. Hwang, and W. L. Mao, Nat. Commun. **6**, 7312 (2015).
[21]S. Duwal and C.-S. Yoo, J. Phys. Chem. C **120**, 5101 (2016).
[22]Z. H. Chi, X. M. Zhao, H. Zhang, A. F. Goncharov, S. S. Lobanov, T. Kagayama, M. Sakata, and X. J. Chen, Phys. Rev. Lett. **113**, 036802 (2014).
[23]A. Jayaraman, Rev. Mod. Phys. **55**, 65 (1983).
[24]L. Dai, H. Hu, H. Li, J. Jiang, and K. Hui, Am. Mineral. **99**, 1420 (2014).
[25]L. Dai, H. Hu, H. Li, L. Wu, K. Hui, J. Jiang, and W. Sun, Geochem. Geophys. Geosyst. **17**, 2394 (2016).
[26]A. Pommier, F. Gaillard, M. Malki, and M. Pichavant, Am. Mineral. **95**, 284 (2010).
[27]A. Pommier, F. Gaillard, and M. Pichavant, Geochim. Cosmochim. Acta **74**, 1653 (2010).
[28]Y. A. Kandrina, A. N. Babushkin, S. N. Shkerin, and Y. Y. Volkova, Defect. Diffus. Forum **208–209**, 295 (2002).
[29]L. Dai, H. Li, H. Hu, and S. Shan, J. Geophys. Res. **113**, B12211, doi:10.1029/2008JB005820 (2008).
[30]O. Gomis, R. Vilaplana, F. J. Manjón, P. Rodríguez-Hernández, E. Pérez-González, A. Muñoz, V. Kucek, and C. Drasar, Phys. Rev. B **84**, 174305 (2011).
[31]W. Ju, T. Li, H. Wang, Y. Yong, and J. Sun, Chem. Phys. Lett. **622**, 109 (2015).
[32]S. Jiménez Sandoval, D. Yang, R. F. Frindt, and J. C. Irwin, Phys. Rev. B **44**, 3955 (1991).
[33]P. E. Kalita, S. V. Sinogeikin, K. Lipinska-Kalita, T. Hartmann, X. Ke, C. Chen, and A. Cornelius, J. Appl. Phys. **108**, 043511 (2010).
[34]R. P. Dias, M. Kim, and C.-S. Yoo, Phys. Rev. B **93**, 104107 (2016).
[35]J. L. Verble and T. J. Wieting, Phys. Rev. Lett. **25**, 362 (1970).
[36]F. Li, Y. Yan, B. Han, L. Li, X. Huang, M. Yao, Y. Gong, X. Jin, B. Liu, C. Zhu, Q. Zhou, and T. Cui, Nanoscale **7**, 9075 (2015).
[37]R. Zallen and M. Slade, Phys. Rev. B **9**, 1627 (1974).
[38]T. J. Wieting and J. L. Verble, Phys. Rev. B **3**, 4286 (1971).
[39]D. Errandonea, A. Muñoz, and J. Gonzalez-Platas, J. Appl. Phys. **115**, 216101 (2014).
[40]Y. Lin, Y. Yang, H. Ma, Y. Cui, and W. L. Mao, J. Phys. Chem. C **115**, 9844 (2011).
[41]L. Fei, S. Lei, W. B. Zhang, W. Lu, Z. Lin, C. H. Lam, Y. Chai, and Y. Wang, Nat. Commun. **7**, 12206 (2016).
[42]A. Polian, M. Gauthier, S. M. Souza, D. M. Trichês, J. Cardoso de Lima, and T. A. Grandi, Phys. Rev. B **83**, 113106 (2011).
[43]Z. Zhao, S. Wang, H. Zhang, and W. L. Mao, Phys. Rev. B **88**, 024120 (2013).
[44]J. Zhang, C. Liu, X. Zhang, F. Ke, Y. Han, G. Peng, Y. Ma, and C. Gao, Appl. Phys. Lett. **103**, 052102 (2013).